

Supplement for “Chemical evolution of primary and secondary biomass burning aerosols during daytime and nighttime”

Amir Yazdani¹, Satoshi Takahama¹, John K. Kodros², Marco Paglione^{2,3}, Mauro Masiol², Stefania Squizzato², Kalliopi Florou², Christos Kaltsonoudis², Spiro D. Jorga², Spyros N. Pandis^{2,4}, and Athanasios Nenes^{1,2}

¹Laboratory of atmospheric processes and their impacts (LAPI), ENAC/IIE, Ecole polytechnique fédérale de Lausanne (EPFL), Lausanne, Switzerland

²Institute for Chemical Engineering Sciences, Foundation for Research and Technology Hellas (ICE-HT/FORTH), Patra, Greece

³Italian National Research Council - Institute of Atmospheric Sciences and Climate (CNR-ISAC), Bologna, Italy

⁴Department of Chemical Engineering, University of Patras, Patra, Greece

Correspondence: Satoshi Takahama (satoshi.takahama@epfl.ch), Athanasios Nenes (athanasios.nenes@epfl.ch)

S1 Size distribution of bbOA

Figure S1a shows the decrease in the OA concentration in a reference experiment (experiment 1). A first-order wall loss can explain the trend of the OA concentration well ($R^2 = 0.8$). The size distribution of OA averaged from -2 to 2 h is shown in Figure S1b. The distribution has its mode close to 200 nm for this experiment and for the majority of other experiments of this study.

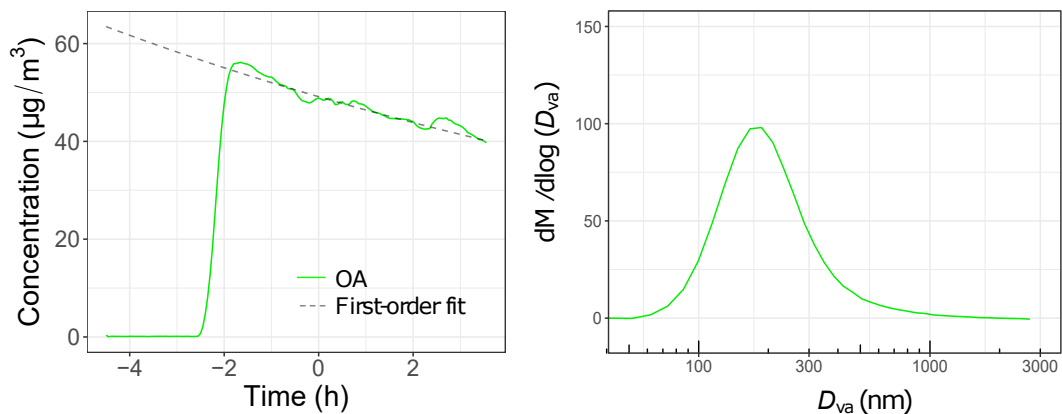


Figure S1. (a) The AMS OA concentration and the first-order fit for Exp. 1 (reference). Injection of biomass burning emissions happens at -2 h. (b) The AMS size-resolved organic mass. The results are based on particle time-of-flight (PToF) data averaged from -2 to 2 h.

S2 Investigating the volatility of lignin-like compounds

In order to estimate the volatility of different species responsible for marker fragments, we assumed that the equilibrium state in gas-particle partitioning is reached at all temperatures and used the equation below:

$$A_i(T) = \frac{G_i(T) + A_i(T)}{1 + C_i^*(T)/M(T)}, \quad (\text{S1})$$

- 10 where $A_i(T)$ and $G_i(T)$ are aerosol-phase and gas-phase concentrations of the fragment i at temperature, T and $M(T)$ denotes the total organic mass. The sum of $A_i(T)$ and $G_i(T)$ are assumed to be the same between the bypass line and the thermodenuder line. The Clausius-Clapeyron equation was used to relate the saturations concentration, C_i^* , at different temperatures:

$$C_i^*(T) = \frac{298}{T} C_i^*(298) \exp \left[\frac{\Delta H_v}{R} \left(\frac{1}{T} - \frac{1}{298} \right) \right]. \quad (\text{S2})$$

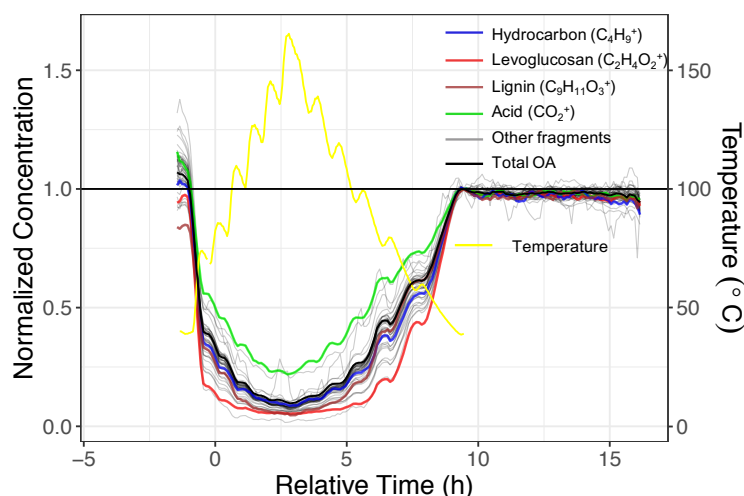


Figure S2. Concentration time series of individual AMS fragments after passing chamber OA through a thermodenuder (normalized by the concentrations through the bypass line). The temperature of the thermodenuder is shown in yellow.

- We neglected particle losses due to thermophoresis. The total organic concentration has been assumed to be the value estimated by AMS considering a CE of unity. ΔH_v is assumed to be equal to 40 kJ mol^{-1} . The Levenberg-Marquardt nonlinear least-Squares algorithm was used to find the optimum C^* for different marker fragments. For $\text{C}_2\text{H}_4\text{O}_2^+$, $\text{C}_9\text{H}_{11}\text{O}_3^+$, $\text{C}_{10}\text{H}_{13}\text{O}_3^+$, CO_2^+ , and C_4H_9^+ , the $C^*(298)$ was estimated to be 5.42, 1.83, 1.32, 0.76, and $2.94 \mu\text{g m}^{-3}$, respectively. The $\text{C}_2\text{H}_4\text{O}_2^+$ is produced by the most volatile species (levoglucosan, anhydrosugars) and the CO_2^+ by the least volatile ones. However the differences are within one order of magnitude for all the fragments above. Due to simplifying assumptions (e.g., omission of thermophoresis or equilibrium state) these values should be considered as order of magnitude estimates. The value of C^* estimated for the levoglucosan is slightly lower than that of Bertrand et al. (2018) but still reasonably when close considering the simplifying assumptions made here.

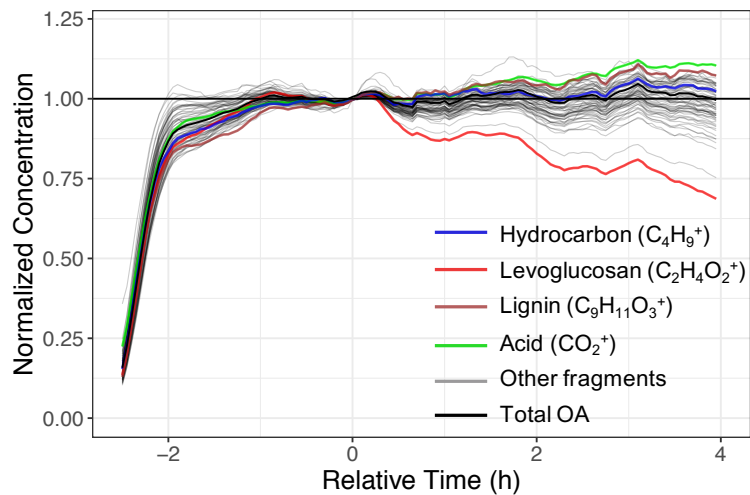


Figure S3. Time series of normalized concentrations of AMS fragments in a reference experiment (Exp. 3).

As can be seen from Fig. S3, a lower loss rate is observed for $C_9H_{11}O_3^+$ in the absence of oxidants compared to other fragments including $C_2H_4O_2^+$. This suggests the lower volatility of the corresponding species as their concentration is mainly affected by particle-phase wall losses compared to particle- and gas-phase wall losses for levoglucosan. This phenomenon is observed in all experiments before the injection of oxidants.

S3 AMS and FTIR comparison

OA concentrations estimated using FTIR and AMS are correlated ($R^2 = 0.75$; Fig. S4). Aging with UV increases the OM:OC ratio more than aging with the nitrate radical. We also observe that the general increase in OM:OC with aging is captured by both methods (Fig. S4c). However, the absolute values are different. PTFE filters that belong to each experiment are as follows: Exp. 1 (filters F1, F2), Exp. 2 (F9, 10), Exp. 3 (F16, 17), Exp. 4 (F18, 19), Exp. 5 (F20, 21), Exp. 6 (F4, 5), Exp. 7 (F11, 12), Exp. 8 (F6, 7), and Exp. (F13, 14). F3, 8, and 18 are blank filters put in the chamber for few minutes. AMS OA is not corrected for the collection efficiency (CE).

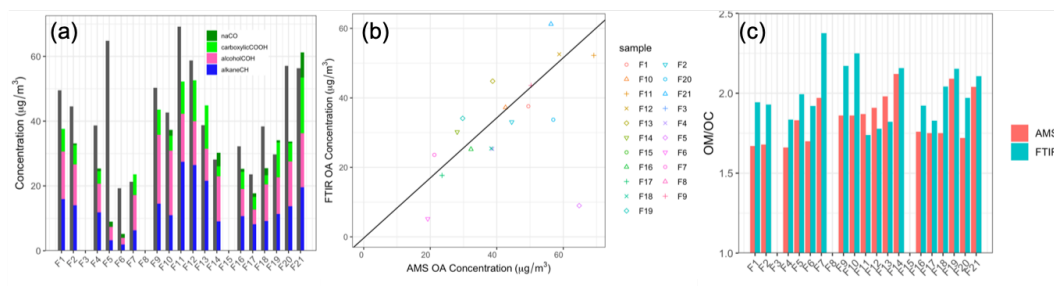


Figure S4. The OA mass concentration measured with FTIR (functional groups are color coded) and AMS (averaged over the filter sampling periods) (a). Scatter plot comparing OA concentrations measured by AMS and FTIR (b). OM:OC ratios measured by AMS and FTIR (c).

S4 Dimension reduction of AMS mass spectra

- 35 In the figure below, the loadings of the first three principal components (up to m/z 73) for an uncentered PCA on the AMS spectra of the chamber experiments are shown. The first PC has high negative loadings of oxygenated fragments ions such as CO^+ , CO_2^+ , CHO^+ , and $\text{C}_2\text{H}_3\text{O}^+$, showing the direction of aging. The CHO^+ fragment has a high positive loading and CO^+ and CO_2^+ have high negative loadings for PC2, suggesting that this PC distinguishes between carboxylic acids which are detected by CO_2^+ and alcohols which produce strong signals of CHO^+ . This is supported by FTIR spectra
- 40 of pellet burning samples which have higher PC2 scores than and strong signatures of the alcohol group than their wood burning counterparts. PC3 has high positive loadings of CO^+ and CO_2^+ and high negative loadings of $\text{C}_2\text{H}_4\text{O}_2^+$, showing the degradation of anhydrosugars with aging.

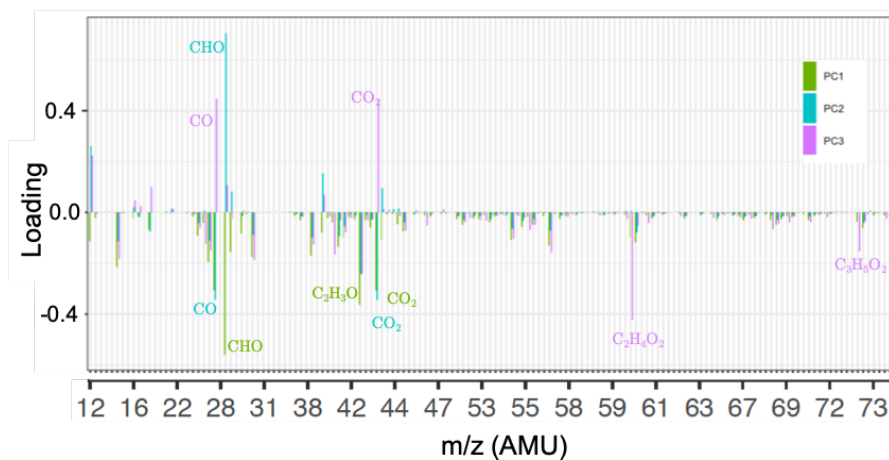


Figure S5. Loadings of the first three PCs.

S5 Ammonium-subtracted spectra

In the figure below ammonium-subtracted residual spectra are shown. Carboxylic acid and alcohol absorbances are clearly observed in these spectra.

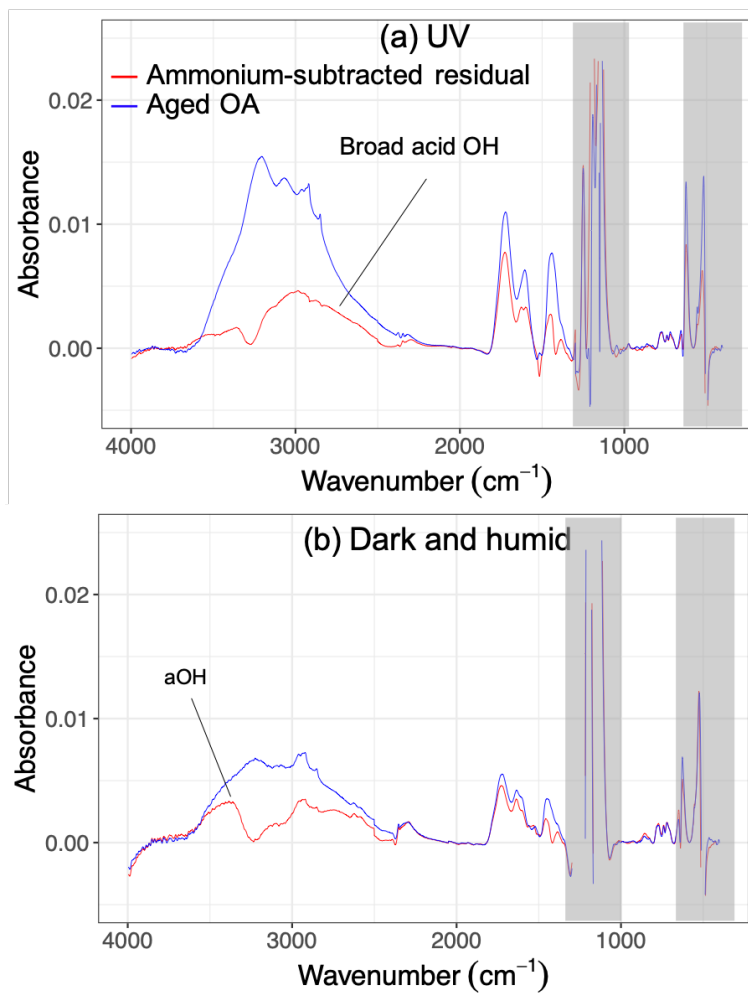


Figure S6. Ammonium-subtracted residual FTIR spectra of wood burning OA aged with UV (a) and nitrate radical (b) (Exp. 4, and 8, respectively).

S6 The FTIR spectrum of atmospheric smoke impacted PM_{2.5}

An example of atmospheric smoke impacted PM_{2.5} samples (prescribed burning in the eastern US in 2013, validated by satellite observations; Yazdani et al., 2021). High organic loading, strong acid signatures, and very weak levoglucosan and invisible lignin-like signatures are observed in the Fig. S7.

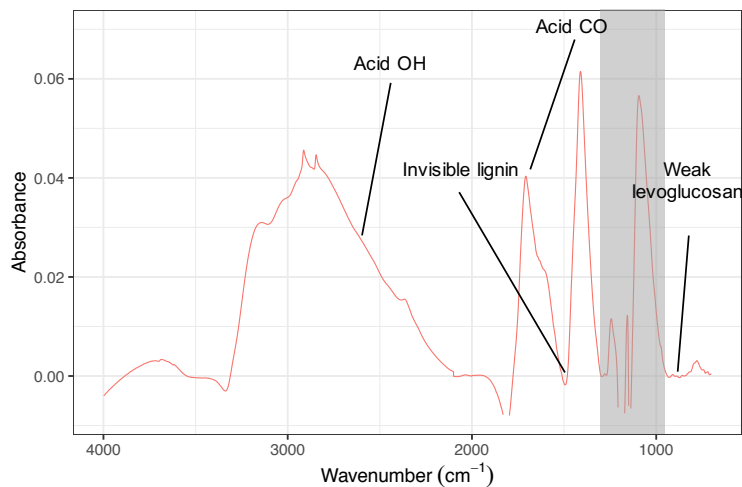


Figure S7. The FTIR spectrum of an atmospheric smoke-impacted PM_{2.5} sample.

50 S7 Loss rates of different fragments

Based on the loss profiles for different fragments within two hours after the initiation of aging (when UV lights are on), the loss rates are estimated to be 0.38, 0.70, 0.24, and 0.23 h^{-1} for $\text{C}_2\text{H}_4\text{O}_2^+$, $\text{C}_9\text{H}_{11}\text{O}_3^+$, $\text{C}_{10}\text{H}_{13}\text{O}_3^+$, and C_4H_9^+ .

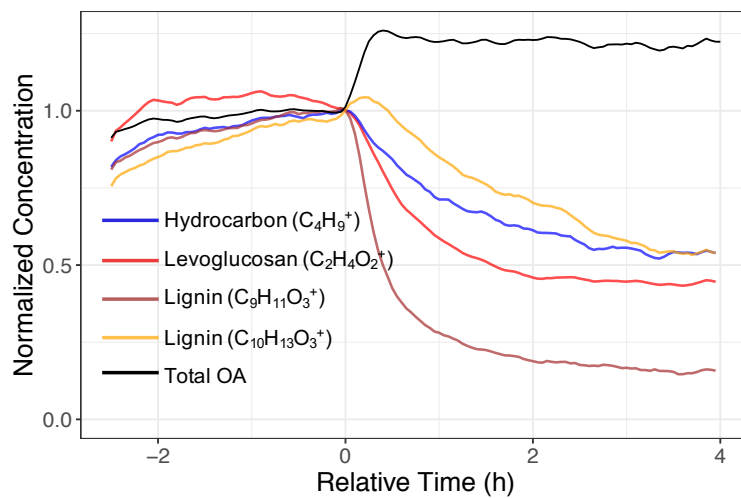


Figure S8. Smoothed time series of AMS OA concentration, and different tracer fragments in a UV experiment (Exp. 4).

S8 $f_{44}:f_{43}$ ratios in residual spectra

In Fig. S9 the wall-loss corrected OA was calculated based on

$$55 \quad C_{\text{OA}}^{\text{cor}}(t) = C_{\text{OA}}^{\text{obs}}(t) + k_{\text{OA}} \int_{t_0}^t C_{\text{OA}}^{\text{obs}}(t) dt, \quad (\text{S3})$$

where $C_{\text{OA}}^{\text{obs}}(t)$ is the observed (measured) OA concentration at time t , $C_{\text{OA}}^{\text{cor}}(t)$ is the wall-loss-corrected OA at the t , k_{OA} is the first-order wall loss rate based on the AMS OA. OC was calculated from the sum of C concentration for all fragments. Dividing OA time series by OM:OC time series gives a similar trend with different absolute values.

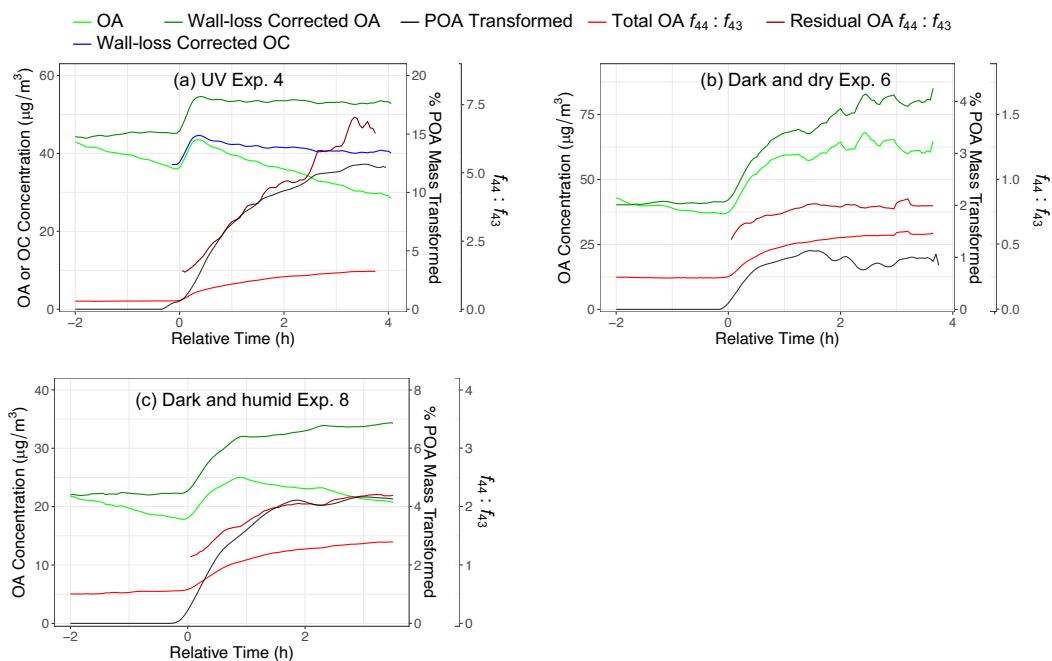


Figure S9. Time series of OA, OC concentrations, percentage of POA mass aged, and $f_{44}:f_{43}$ for wood burning emissions in different aging scenarios.

As can be seen from Fig. S9, the trends of POA aging and $f_{44}:f_{43}$ are similar in different experiments. The decrease in the
 60 OC concentration in the UV experiment with aging suggests the importance of other aging mechanisms such as photolysis in addition to the SOA condensation.

References

- Bertrand, A., Stefenelli, G., Pieber, S. M., Bruns, E. A., Temime-Roussel, B., Slowik, J. G., Wortham, H., Prévôt, A. S. H., Haddad, I. E., and Marchand, N.: Influence of the Vapor Wall Loss on the Degradation Rate Constants in Chamber Experiments of Levoglucosan and Other Biomass Burning Markers, *Atmos. Chem. Phys.*, 18, 10915–10930, <https://doi.org/10.5194/acp-18-10915-2018>, 2018.
- 65 Yazdani, A., Takahama, S., Raffuse, S., Dillner, A. M., and Sullivan, A. P.: Identification of Smoke-Impacted PM_{2.5} Samples with Mid-Infrared Spectroscopy in a Monitoring Network, Manuscript in preparation, 2021.